Clim Dyn (2018) 50:2753–2765
DOI 10.1007/s00382-017-3769-8

A new index for identifying different types of El Niño Modoki events

Xin Wang[1,2] · Wei Tan[3] · Chunzai Wang[1]

Received: 27 December 2016 / Accepted: 10 June 2017 / Published online: 23 June 2017

Abstract El Niño Modoki events can be further classified into El Niño Modoki I and II in terms of their opposite impacts on southern China rainfall (Wang and Wang, J Clim 26:1322–1338, 2013) and the Indian Ocean dipole mode (Wang and Wang, Clim Dyn 42:991–1005, 2014). The present paper develops an index to identify the types of El Niño events. The El Niño Modoki II (MII) index is defined as the leading principle component of multivariate empirical orthogonal function analysis of the normalized El Niño Modoki index, Niño4 index and 850 hPa relative vorticity anomalies averaged near the Philippine Sea during autumn. The MII index exhibits dominant variations on interannual (2–3 and 4–5 years) and decadal (10–20 years) timescales. El Niño Modoki II events can be well identified by using the MII index value being larger than 1 standard deviation. Further analyses and numerical model experiments confirm that the MII index can portray the major oceanic and atmospheric features of El Niño Modoki II events. The constructed MII index along with previous ENSO indices can be used for classifying and identifying all types of El Niño events. Because of distinct impacts induced by different types of El Niño events, the implication of the present study is that climate prediction and future climate projection under global warming can be improved by using the MII index and other indices to identify the types of El Niño events.

Keywords ENSO · El Niño Modoki · Climate impacts

1 Introduction

El Niño-Southern Oscillation (ENSO), as a coupled ocean–atmosphere phenomenon, is a prominent signal in the tropical Pacific, and plays a critical role in climate variability (Bjerknes 1966, 1969; Rasmusson and Carpenter 1982; Jin 1997; Trenberth 1997; Weisberg and Wang 1997; Wang et al. 2000, 2016; Alexander et al. 2002; Wang 2002). During El Niño, the western Pacific warm pool extends eastward and warm sea surface temperature (SST) anomalies thus appear in the equatorial eastern and central Pacific. Motivated by this significant feature, the SST anomalies averaged in the tropical eastern or central Pacific are conventionally used to characterize El Niño, such as Niño3 index (150–90°W, 5°S–5°N), Niño4 index (160°E–150°W, 5°S–5°N), Niño3.4 index (170–120°W, 5°S–5°N) and Niño1 + 2 index (90–80°W, 0°–10°S). In response to the SST anomalies, the sea level pressure (SLP) anomalies exhibit the so-called Southern Oscillation pattern of high (low) SLP anomalies over the equatorial western (eastern) Pacific (Bjerknes 1969). Accordingly, El Niño can be also identified by the Southern Oscillation index (SOI), which is calculated as the SLP differences between Tahiti and Darwin (Ropelewski and Jones 1987). Moreover, the zonal shift of the western Pacific warm pool can be described by the longitudinal location of the sea surface salinity (SSS) front along the equator (Delcroix and Picaut 1998; Picaut et al. 2001; Singh et al. 2011), and it thus is an

✉ Chunzai Wang
cwang@scsio.ac.cn

[1] State Key Laboratory of Tropical Oceanography, South China Sea Institute of Oceanology, Chinese Academy of Sciences, 164 West Xingang Road, Guangzhou 510301, China

[2] Laboratory for Regional Oceanography and Numerical Modeling, Qingdao National Laboratory for Marine Science and Technology, Qingdao 266237, China

[3] First Institute of Oceanography, State Oceanic Administration, Qingdao 266061, China

excellent El Niño indicator as well. Trenberth and Stepaniak (2001) developed a Trans-Niño index (TNI) to portray the evolution of El Niño, which is constructed by the normalized SST anomaly difference between the Niño1 + 2 and Niño4 regions. All of these above-mentioned indices are based on a single variable.

In addition, according to the coupled ocean–atmosphere responses to El Niño, there are also other indices on the basis of multiple variables, such as multivariate ENSO index (MEI) (Wolter and Timlin 1993), extended MEI (MEI.ext) (Wolter and Timlin 2011), and the coupled ENSO index (CEI) (Gergis and Fowler 2005). Using multivariate empirical orthogonal function (MV-EOF) analysis of the combined oceanic and atmospheric variables, Wang and Wang (1994) showed that the leading mode of MV-EOF exhibits the mature phase of El Niño. The second mode displays the equatorial central Pacific warming, and it is considered as the developing (early warming) phase of El Niño. Besides, there are some other proxy-based ENSO indices using fossil coral, tree ring, and ice core record (Cobb et al. 2003; Braganza et al. 2009), and they are usually applied in a more distant past.

In recent years, more and more literatures have regarded the central Pacific warming as a new type of El Niño, which is alternatively called Dateline El Niño (Larkin and Harrison 2005), El Niño Modoki (Ashok et al. 2007), central Pacific (CP) El Niño (Kao and Yu 2009), or warm pool El Niño (Kug et al. 2009). In this study, the name of "El Niño Modoki" is used for the warming SST anomalies in the central Pacific. In the past three decades, the occurrence frequency and intensity of El Niño Modoki are increasing (Ashok et al. 2007; Yeh et al. 2009; Lee and McPhaden 2010). Owing to the differences of warming SST anomaly distributions and intensities between canonical El Niño and El Niño Modoki, there exist substantial discrepancies in anomalous large-scale atmospheric circulations and the associated climate influences (Ashok et al. 2007; Weng et al. 2007; Kao and Yu 2009; Kug et al. 2009; Hong et al. 2011; Kim et al. 2012; Liu et al. 2014; Wang et al. 2014).

In order to distinguish two types of El Niño, several indices have been proposed. Based on the empirical orthogonal function (EOF) analysis of the SST anomalies in the tropical Pacific, Ashok et al. (2007) found that the first two EOF modes could capture the geographical patterns of two types of El Niño well. The second EOF mode exhibits a zonal tripole structure, i.e., warmer SST anomalies locate in the central equatorial Pacific flanked by colder SST anomalies in the eastern and western Pacific. Due to the differences of SST anomalies in these three regions, an El Niño Modoki index (EMI) is defined as:

$$EMI = [SSTA]_C - 0.5 \times [SSTA]_W - 0.5 \times [SSTA]_E, \quad (1)$$

where the brackets indicate the SST anomalies averaged in Regions C (165°E–140°W, 10°S–10°N), W (125–145°E, 10°S–20°N), and E (110–70°W, 15°S–5°N), respectively (red boxes in Fig. 1).

Through a combined regression-EOF analysis, Kao and Yu (2009) first removed the tropical SST anomalies regressed with Niño1 + 2 index and Niño4 index linearly, and then considered the leading principle component (PC-1) of the EOF to the residual SST anomalies as CP El Niño index and canonical El Niño index, respectively. Likewise, using the same method, the regression with Niño3 index instead of Niño1 + 2 index is removed before the EOF for a CP El Niño index calculation (Di Lorenzo et al. 2010). The EOF is also performed by Takahashi et al. (2011), and the first two principle components (PC-1 and PC-2) are both rotated 45° clockwise to construct an E-index (representing canonical El Niño) and a C-index (representing El Niño Modoki), respectively. In addition, the two types of El Niño can be distinguished by contrasting the magnitudes of the Niño3 and Niño4 indices (Kug et al. 2009; Yeh et al. 2009). Based on this method, Ren and Jin (2011) further redefined a canonical El Niño index (N_{CT} index) and an El Niño Modoki index (N_{WP} index) through a nonlinear transformation of Niño3 and Niño4 indices. The N_{CT} and N_{WP} indices show a weak correlation. Besides the SST anomalies, the subsurface ocean temperature anomalies in the tropical eastern (80–90°W, 5°S–5°N) and central Pacific (160°E–150°W, 5°S–5°N) are also utilized as two types of El Niño indices (Yu et al. 2011). Moreover, the SSS anomalies in the tropical southeastern Pacific (150–90°W, 0°–10°S) are also found to represent El Niño Modoki events (Qu and Yu 2014). The outgoing longwave radiation (OLR) anomalies in the eastern-to-central equatorial Pacific (160–110°W, 5°S–5°N) can divide El Niño events into OLR El Niño and non-OLR El Niño events (Chiodi and Harrison 2013). These indices are summarized in Table 1 [also see Capotondi et al. (2015)].

El Niño Modoki events can be further divided into El Niño Modoki I and II in terms of their different influences

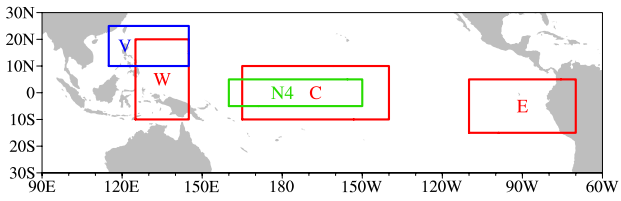

Fig. 1 Spatial domains for the calculation of the EMI (*red boxes* with *W, C, E*), Niño4 index (*green box* with N4), and the relative vorticity anomalies at 850 hPa (*blue box* with *V*). Regions *W, C*, and *E* are in the areas of (125–145°E, 10°S–20°N), (165°E–140°W, 10°S–10°N), and (110–70°W, 15°S–5°N), respectively. *N4 box* is in the area of (160°E–150°W, 5°S–5°N,), and *V box* is in the region of (115–145°E, 10–25°N)

Table 1 Summary of the El Niño Modoki indices used in previous studies

Definitions	References
$EMI = [SSTA]_C - 0.5 \times [SSTA]_W - 0.5 \times [SSTA]_E$	Ashok et al. (2007)
Niño4 > 1 STD Niño4 > Niño3	Kug et al. (2009); Yeh et al. (2009)
PC-1 of the EOF to the residual SST anomalies after removing the regressed SST anomalies with Niño1 + 2 index	Kao and Yu (2009)
PC-1 of the EOF to the residual SST anomalies after removing the regressed SST anomalies with Niño3 index	Di Lorenzo et al. (2010)
$N_{WP} = \text{Niño4} - \text{Niño3}, \boldsymbol{\alpha} = \begin{cases} 2/5, & Niño3 \times Niño4 > 0 \\ 0, & otherwise \end{cases}$	Ren and Jin (2011)
PC-2 rotated 45° clockwise of SST (C-index)	Takahashi et al. (2011)
Temperature anomalies in the upper 100 m averaged in the central Pacific (160°E–150°W, 5°S–5°N)	Yu et al. (2011)
Outgoing longwave radiation (OLR) anomalies averaged in the eastern-to-central equatorial Pacific (160°W–110°W, 5°S–5°N), which is used to identify OLR El Niño event	Chiodi and Harrison (2013)
Southeastern Pacific SSS index (SEPSI) averaged in the region (150–90°W, 0°–10°S)	Qu and Yu (2014)

$[SSTA]_C$, $[SSTA]_W$, and $[SSTA]_E$ are the SST anomalies averaged in (165°E–140°W, 10°S–10°N), (125–145°E, 10°S–20°N), and (110–70°W, 15°S–5°N), respectively. Niño4, Niño3 and Niño1 + 2 mean the SST anomalies averaged in (160°E–150°W, 5°S–5°N), (150–90°W, 5°S–5°N), and (90–80°W, 0°–10°S)

STD standard deviation

on rainfall in southern China during boreal autumn (Wang and Wang 2013). El Niño Modoki I (II) is identified when the autumn-averaged (Sept–Oct–Nov, SON) rainfall anomalies in southern China are more (less) than the normal. Moreover, El Niño Modoki I and II exhibit distinct spatial–temporal evolutions of SST anomalies during the developing stage. For El Niño Modoki I, the anomalous warm SST originates in the equatorial central Pacific, and the warming region is confined locally. While during El Niño Modoki II, the anomalous warm SST initially emerges in the subtropical northeastern Pacific, and then extends southwestward to the equatorial central Pacific (Wang and Wang 2013). Due to such different geographic distributions of SST anomalies, El Niño Modoki I and II have significantly distinct impacts on the typhoon tracks (Wang and Wang 2013), the Indian Ocean Dipole (IOD) (Wang and Wang 2014) and SST in the South China Sea (SCS) during boreal autumn (Tan et al. 2016). All of these studies use the El Niño Modoki I and II events defined by Wang and Wang (2013) to perform the composite analyses or model experiments. However, an index for identifying El Niño Modoki I and II events does not yet exist. The purpose of the present paper is to develop a new index for identifying El Niño Modoki II events (MII index) according to the associated ocean–atmosphere features. Using MII index and EMI, we can objectively identify El Niño Modoki I and II events. The new index for identifying El Niño Modoki I and II events has an important implication for climate prediction and typhoon seasonal outlook since they have different rainfall distributions in southern China and different typhoon landfall activities.

The rest of the paper is organized as follows. Section 2 presents a brief introduction of the data sets, methods and model used in the study. The MII index is constructed in Sect. 3, followed by large-scale circulations associated with MII index in Sect. 4. Numerical model simulations are performed in Sect. 5 in association with for the constructed MII index. Finally, a summary and discussion is given in Sect. 6.

2 Data sets, methods and numerical model

2.1 Data sets

The monthly Hadley Centre Sea Ice and SST (HadISST) data set (Rayner et al. 2003) and the atmospheric reanalysis data set from the National Centers for Environmental Prediction/National Center for Atmospheric Research (NCEP/NCAR) (Kalnay et al. 1996) are used in the study. The HadISST data set has a spatial resolution of 1°×1° from 1870 to 2016, and the NCEP/NCAR reanalysis with a horizontal resolution of 2.5° × 2.5° and 17 vertical levels covers from 1948 to 2016. The gridded monthly data set of rainfall is provided by the Global Precipitation Climatology Centre (GPCC) with a resolution of 1° × 1° from 1901 to present (Schneider et al. 2011) for the MII index validation, which is available from http://www.esrl.noaa.gov/psd/data/gridded/data.gpcc.html. In addition, the Niño3 and Niño4 indices used in this study are obtained from National Oceanic

and Atmospheric Administration (NOAA)/Earth System Research Laboratory (ESRL) from 1950 to present.

We firstly removed the linear trend before analyses, and all of the anomalies are calculated as departures from 1971 to 2000 climatology. In this study, the Niño3 index is used to depict canonical El Niño, and the EMI index is employed to identify El Niño Modoki events (including El Niño Modoki I and II).

2.2 Methods and numerical model

In this study, an MV-EOF analysis (Wang 1992; Wang and Wang 1994; Wang et al. 2008) is applied to construct the MII index. The MV-EOF extends the traditional EOF for a single variable utilizing the coherence of multiple variables, which has notable advantages in depicting the coherent variation of multiple variables simultaneously and portraying the coupled ocean–atmosphere processes well (Wang 1992). In addition, the power spectral analysis, correlation analysis ("Appendix"), and linear regression analysis are also used in the study.

To further confirm El Niño Modoki events defined by the constructed MII index, we conduct model experiments by using the Community Atmosphere Model version 4 (CAM4, Neale et al. 2013). Composited SST anomalies of El Niño Modoki I and II events identified in the study are used to drive CAM4, and the simulated atmospheric responses are compared with the observation for a verification. As the sixth generation of the atmospheric general circulation model (AGCM), CAM4 is the atmospheric component of the Community Climate System Model version 4 (CCSM4) (Gent et al. 2011). Dynamical core, deep convective parameterization and cloud fraction calculation in CAM4 have been significantly improved compared with previous versions (Neale et al. 2013). Here, the default finite volume dynamical core is applied, and a coarse spatial resolution of 3.75° × 3.75° with 26 vertical levels is used.

3 Construction of the MII index

Although the warm SST anomalies reach peak in the equatorial central Pacific during boreal winter (Dec-Jan-Feb, DJF) of both El Niño Modoki I and II, the origins and evolutions are quite different (Fig. 2). For El Niño Modoki II, the anomalous warm SST first emerges in the subtropical northeastern Pacific, and then develops and extends southwestward to the equatorial central Pacific (Fig. 2c). In contrast, for El Niño Modoki I, the anomalous warm SST appears in the tropical central Pacific and develops locally (Fig. 2b). Thus, El Niño Modoki I resembles "El Niño Modoki" (Ashok et al. 2007) which is associated with the thermocline deepening in the central equatorial Pacific caused by the wind distribution of the El Niño event. However, El Niño Modoki II is more analogous to "CP El Niño" (Kao and Yu 2009), which corresponds to positive surface heat flux anomalies in the subtropical northeastern Pacific and indicates the impacts of extratropical climate systems on the tropics (Yu et al. 2010; Yu and Kim 2011). Hence, the dynamical connections of El Niño Modoki I and II with the extratropical climate variability may be different and need to be further studied in the future. These temporal-spatial evolutions are consistent with those in Wang and Wang (2013), and the substantial discrepancies are distinctly observed in boreal autumn. The warm SST anomalies are symmetric about the equator during fall of El Niño Modoki I, while they are asymmetric (almost in the north of the equator) for El Niño Modoki II, and stretch farther westward in the equatorial central Pacific compared with El Niño Modoki I (Wang and Wang 2013). Forced by such different SST anomalies, the corresponding atmospheric responses are significantly different in autumn. An anomalous cyclone is located over the Philippine Sea associated with a strongly positive relative vorticity at low level during fall of El Niño Modoki II (Fig. 2c), while for El Niño Modoki I, an anomalous anticyclone with low-level negative wind vorticity is found near the Philippine Sea in SON (Fig. 2b). This atmospheric response during El Niño Modoki I resembles that of canonical El Niño (Fig. 2a).

Considered the patterns of anomalous warm SST in the equatorial central Pacific and anomalous anticyclone/cyclone over the western North Pacific in fall of El Niño Modoki I/II, we perform an MV-EOF analysis by using the normalized autumn-averaged EMI, Niño4 index (green box in Fig. 1), and the relative vorticity anomalies at 850 hPa averaged in the Philippine Sea (115–145°E, 10–25°N; blue box in Fig. 1) during SON.

The first MV-EOF mode accounts for 67.7% of the total variance, and exceeds 95% significance (North et al. 1982). The first mode of the EMI, Niño4 index, and anomalous relative vorticity is 0.67, 0.60 and 0.43, respectively. This indicates that when an El Niño Modoki event occurs, the tropical central Pacific is warm and positive relative vorticity anomalies associated with an anomalous cyclone appear over the Philippine Sea. The first mode can well capture the basic pattern and feature of El Niño Modoki II. Thus, the first principle component (PC-1) of the MV-EOF mode is defined as the MII index in this paper (Fig. 3).

Power spectral analysis of the MII index shows significant interdedadal variations (10–20 years) and interannual variations (2–3 and 4–5 years) (Fig. 4), which is consistent with previous studies of CP El Niño (Weng et al. 2007; Kao and Yu 2009; Xu et al. 2012). We also use the wind field data sets from the Twentieth-Century Reanalysis (20CR) (Compo et al. 2011) and ERA-Interim (Dee et al. 2011)

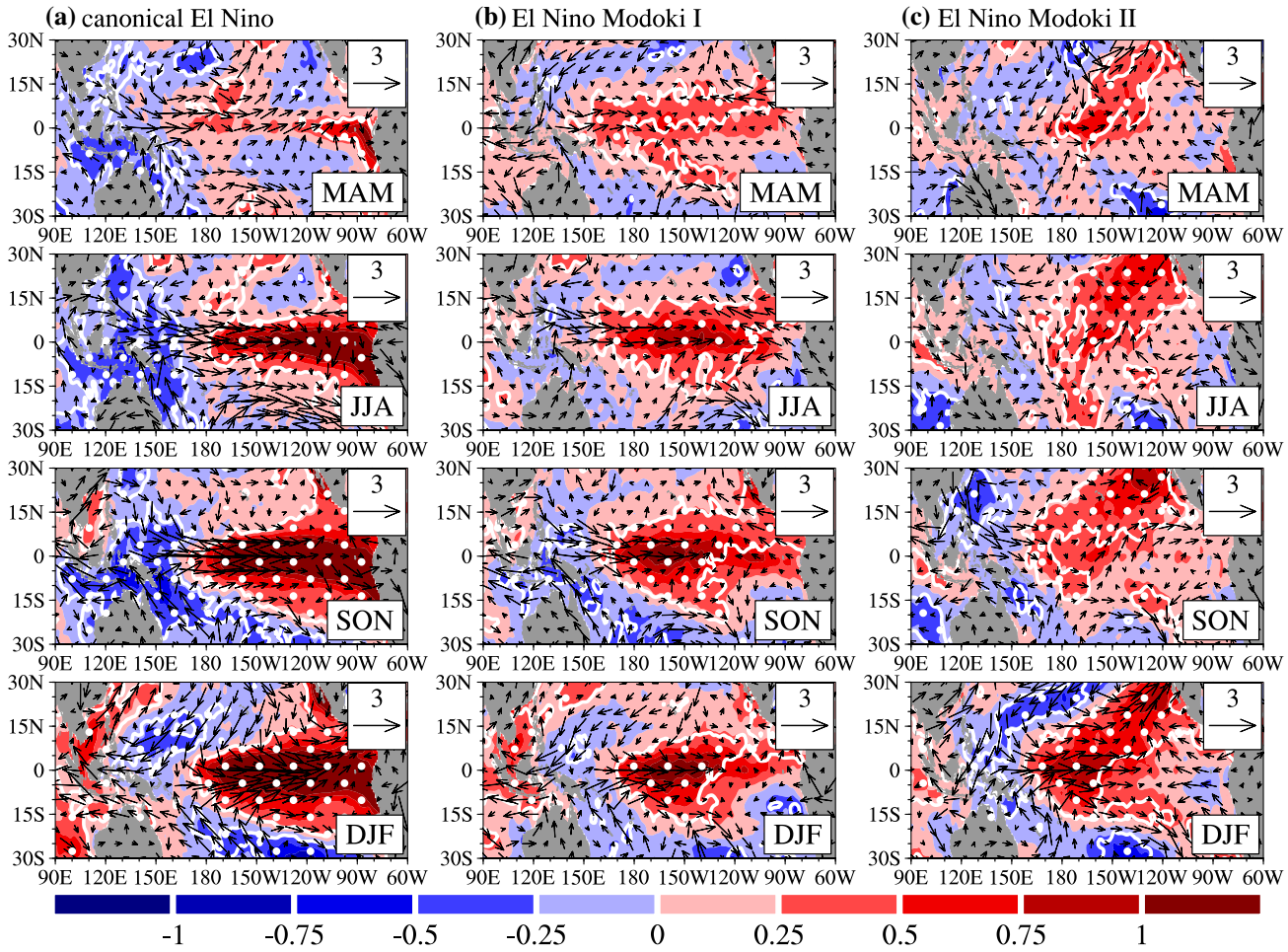

Fig. 2 Evolution of composited SST anomalies (*shading*; °C) and 850 hPa wind anomalies (*vector*; m s^{-1}) during canonical El Niño (**a**; *left column*), El Niño Modoki I (**b**; *middle column*) and El Niño Modoki II (**c**; *right column*) from boreal spring (Mar–Apr–May, MAM) to winter (Dec–Jan–Feb, DJF). The *white contours filled with dots* represent the composite exceeding the 90% significance level based on Student's t test. The HadISST dataset and NCEP/NCAR reanalysis are used for SST and wind, respectively. The El Niño years are selected according to Wang and Wang (2013)

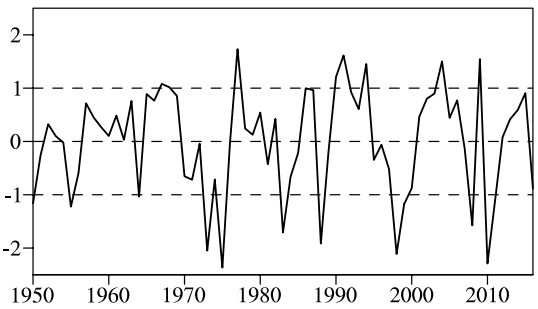

Fig. 3 Time series of the normalized MII index. The *dashed lines* represent 0 and ±1 standard deviation

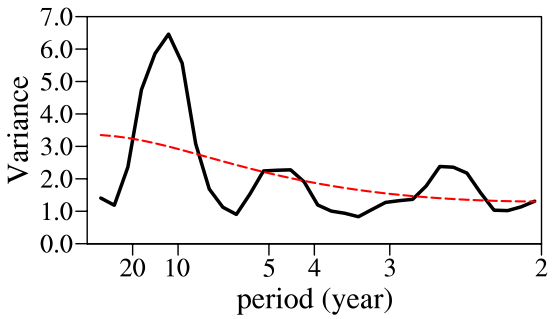

Fig. 4 The power spectrum of the MII index (*black line*) and the associated Markov red noise spectrum (*red dashed line*)

Table 2 Correlation coefficients of the MII index with the Niño3 index, Niño4 index, EMI, and N_{WP} index in autumn (SON) and winter (DJF)

	SON				DJF			
	Niño3	Niño4	EMI	N_{WP}	Niño3	Niño4	EMI	N_{WP}
MII	***0.54***	***0.86***	***0.95***	***0.90***	***0.56***	***0.82***	***0.88***	***0.85***

The numbers in bold and italic indicate the correlation coefficients exceeding the 99% significant level (larger than 0.32)

Table 3 Years of El Niño Modoki II warm and cold events chosen by the normalized MII index larger than 1 (left column) and less than −1 (right column) during 1950–2016

MII > 1	MII < −1
1967	1950
1968	1955
1977	1964
1990	1973
1991	1975
1994	1983
2004	1988
2009	1998
	1999
	2008
	2010
	2011

Table 4 Years of El Niño Modoki, El Niño Modoki I and El Niño Modoki II

El Niño Modoki	El Niño Modoki I	El Niño Modoki II
1963	1963	
1968		1968
1977		1977
1979	1979	
1987	1987	
1990		1990
1991		1991
1992	1992	
1994		1994
2002	2002	
2004		2004
2009		2009

El Niño Modoki events are identified by the EMI (left column), El Niño Modoki II events are identified by the MII index (right column), and the rests are El Niño Modoki I (middle column)

to perform the MV-EOF analysis along with the HadISST. These MII indices are highly correlated with each other (correlation coefficients are up to 0.99), confirming that the MII index is independent of data sets.

The correlation coefficients of the MII index with Niño3, Niño4, EMI, and N_{WP} indices all exceed the 99% significant level (Table 2). Among these indices, the MII index is highly correlated with the Niño4, EMI, and N_{WP} indices, especially for the autumn-averaged EMI and N_{WP} indices (the correlation coefficients are above 0.9). Moreover, the MII index is also related to the Niño3 index (with the correlations of 0.54 and 0.56 in SON and DJF, respectively), indicating its connection with eastern Pacific warming events.

El Niño Modoki II events can be identified through the MII index. An El Niño Modoki II event is identified when the value of the MII index is greater than 1 standard deviation. Based on this criterion, eight cases (1967, 1968, 1977, 1990, 1991, 1994, 2004, and 2009) are selected (Table 3). Compared with El Niño Modoki events (Table 4) identified by the EMI (Ashok et al. 2007), seven of these eight cases (1968, 1977, 1990, 1991, 1994, 2004, and 2009) belong to El Niño Modoki. The exception is 1967 which is a La Niña episode. Therefore, these seven cases are marked as the developing years of El Niño Modoki II. Two of these seven cases (1977 and 1994) are not included in Wang and Wang (2013). It should be noted that El Niño Modoki II events are initially defined as the years when the autumn-averaged rainfall anomalies in southern China are below −0.5 standard deviations (Wang and Wang 2013). However, for 1977 and 1994, the rainfall anomalies are so close to -0.5 standard deviations (Fig. 2 in Wang and Wang 2013), and thus these 2 years should be recognized as weak El Niño Modoki II events. In comparison with Wang and Wang (2013), two cases of 1979 and 1992 are not shown by the MII index. It is noted that the El Niño Modoki II events in Wang and Wang (2013) are separated based on their different climate impacts in China. However, the El Niño Modoki II events from the MII index in the study are based on the ocean–atmosphere characteristics. Due to the method and definition differences, it is not surprising that all of the identified El Niño Modoki II years are not exactly same. Actually, seven El Niño Modoki II years identified by the MII index since 1950 are more objective and reliable. Among all these seven cases, five El Niño Modoki II events occur after 1990, which may be related to the increased influence of the North Pacific on the tropical Pacific since 1990 (Yu et al. 2012; Yeh et al. 2015). Moreover, the same cases are exactly obtained by the MII index calculated by the wind field from the 20CR and ERA-Interim (ERA-Interim is available from

1979, thus only the events after 1979 are considered for ERA-Interim). On the other side, 12 events identified as La Niña by NOAA/Climate Prediction Center (CPC) can also be picked out when the MII index is less than −1 standard deviation (Table 3).

In a short summary, the new index can be used to separate El Niño Modoki events. All of El Niño Modoki events (both El Niño Modoki I and II) can be first identified by the EMI index (Ashok et al. 2007). El Niño Modoki II events are selected by the MII index. Subtracting El Niño Modoki II events from all of El Niño Modoki events gives rise to El Niño Modoki I events. Using this method, El Niño Modoki I and II can be readily classified (Table 4), and the seasonal evolutions of composited SST anomalies during El Niño Modoki I and II (Fig. 5) are similar to Fig. 2.

4 Large-scale circulations associated with MII

The constructed MII index can be used to separate El Niño Modoki I and II events. Here we compare the large-scale circulations of El Niño Modoki I and II based on the MII index. Since the MII index is closely related to the Niño3 and EMI indices (Table 2), the partial correlation analysis is utilized ("Appendix"). After removing the influences of the EMI and Niño3 indices, the MII index is not significantly correlated with the autumn-averaged SST anomalies in the equatorial Pacific, while the correlation still keeps

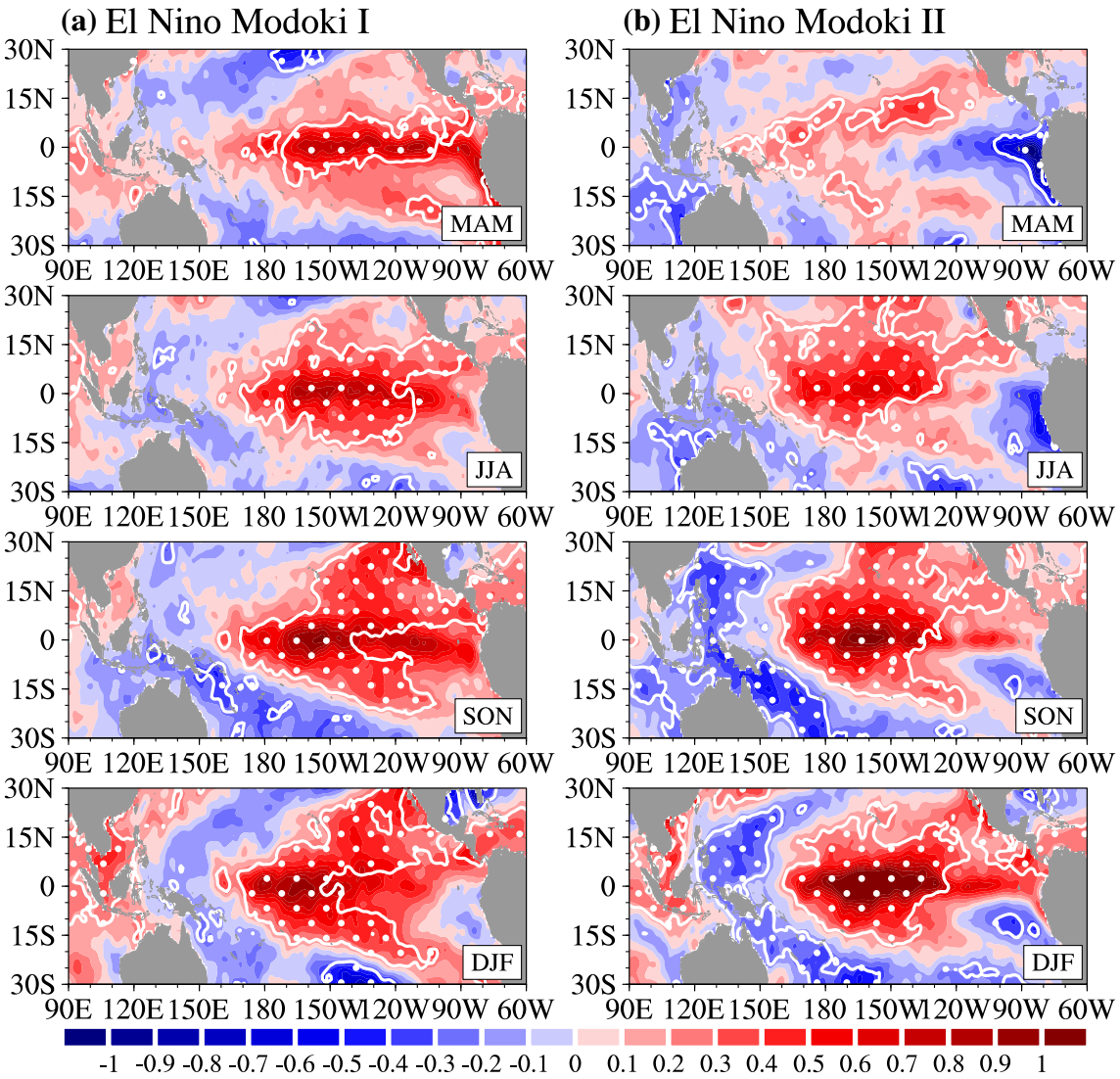

Fig. 5 Evolution of composited SST anomalies (°C) used the identified El Niño Modoki I (**a**; *left column*) and El Niño Modoki II (**b**; *right column*) from boreal spring (MAM) to winter (DJF). The *white contours filled with dots* represent the composite exceeding the 90% significance level based on Student's t test. The El Niño years are used from Table 4

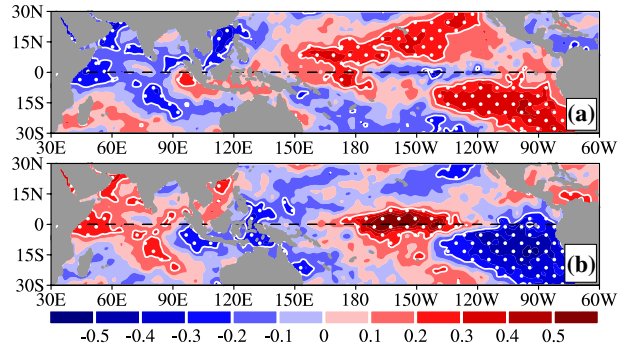

Fig. 6 Partial correlation patterns between the SST anomalies and the MII index (after removing the influences of EMI and Niño3 indices) (**a**), and between the SST anomalies and EMI (after removing the influences of MII and Niño3 indices) (**b**) during boreal autumn. The correlation exceeding the 90% confidence level is enclosed by the *white contours filled with dots*

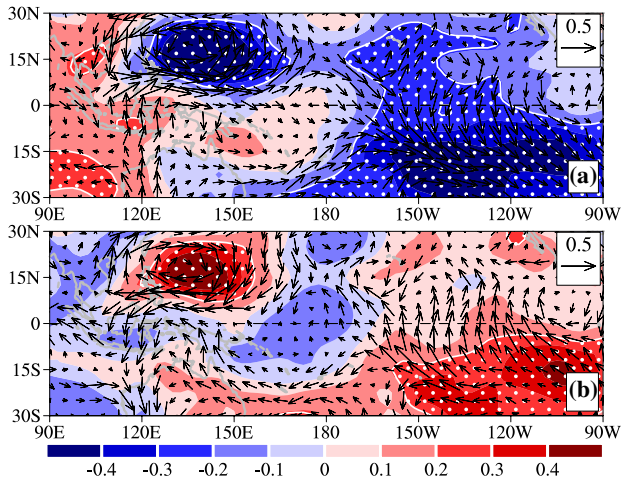

Fig. 7 Partial correlation patterns of 850 hPa wind anomalies (*vector*) and SLP anomalies (*shading*) with the MII index (after removing the influences of Niño3 and EMI indices) (**a**) and with EMI (after removing the influences of MII and Niño3 indices) (**b**) during boreal autumn. The correlation with the SLP anomalies exceeding the 90% confidence level is enclosed by the *white contours filled with dots*

substantially positive in the subtropical northeastern Pacific (Fig. 6a). It should be noted that this anomalous warm SST distribution for El Niño Modoki II is the outstanding characteristic distinguished from El Niño Modoki I suggested by Wang and Wang (2013). A negative correlation is found in the SCS and western North Pacific, which is in accordance with the SCS SST cooling during autumn of El Niño Modoki II (Tan et al. 2016). In the Indian Ocean, there is a positive correlation in the tropical eastern Indian Ocean off Java-Sumatra, but a negative correlation in the tropical central-western Indian Ocean (Fig. 6a). This is consistent with the results of Wang and Wang (2014) that El Niño Modoki II is in favor of the appearance of a negative IOD.

In contrast, the partial correlation between the EMI and the SST anomalies (after removing the influences of the MII and Niño3 indices) in autumn primarily reflects the spatial pattern of El Niño Modoki I (Fig. 6b). The remarkably positive correlation is concentrated in the tropical central Pacific accompanying with negative correlations in the eastern and western tropical Pacific. The Indian Ocean presents a positive IOD-like pattern with negative correlation in the eastern Indian Ocean off Java-Sumatra, and positive correlation in the tropical central-western Indian Ocean (Wang and Wang 2014).

Similarly, the partial correlations of the MII and EMI indices with the atmospheric circulations also portray the atmospheric responses to El Niño Modoki II and I, respectively. The MII index shows a negative correlation with the SLP anomalies and an anomalous cyclone circulation at 850 hPa over the western North Pacific (Fig. 7a). In contrast, a significantly positive correlation exists over the western North Pacific between the EMI and SLP anomalies and an anomalous anticyclone circulation is located in the western North Pacific (Fig. 7b). The anomalous cyclone and anticyclone in the western North Pacific during El Niño developing autumn induce different atmospheric circulations and thus different climate impacts.

An important impact of El Niño Modoki I and II events is different patterns of rainfall in China (Wang and Wang

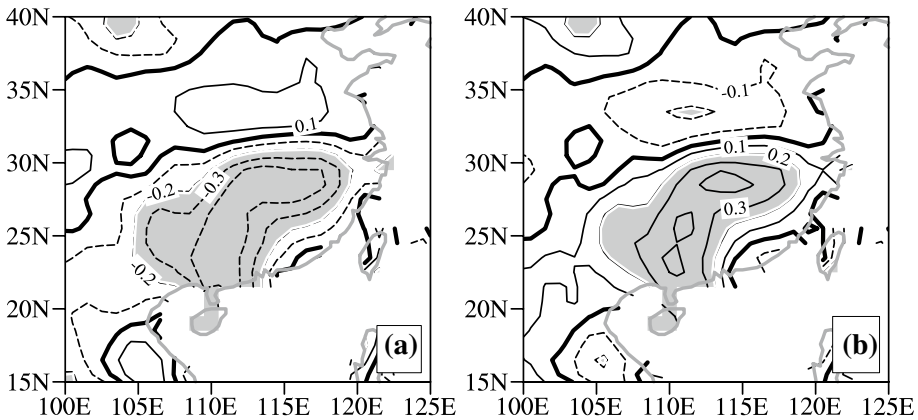

Fig. 8 Partial correlation patterns of anomalous rainfall with the MII index (after removing the influences of EMI and Niño3 indices) (**a**) and with EMI (after removing the influences of MII and Niño3 indices) (**b**) during boreal autumn. The *solid and dashed contours* mean positive and negative correlations with 0.1 contour interval, respectively. The zero contour lines are *thickened*. The correlations exceeding the 90% confidence level are *shaded*

2013). The rainfall in southern China (south of 30°N) during autumn is negatively correlated with the MII index after removing the influences of EMI and Niño3 indices (Fig. 8a), while it is positively correlated with EMI without the influences of the MII and Niño3 indices (Fig. 8b). This result is consistent with the composite precipitation as discussed in Wang and Wang (2013), i.e., the rainfall in southern China decreases and increases in boreal autumn for El Niño Modoki II and I, respectively. All of the above analyses (Figs. 6, 7, 8) provide the evidence that the MII index can well portray the coupled ocean–atmosphere response to El Niño Modoki II events, which have great differences with these to El Niño Modoki I events (and canonical El Niño events).

5 Model experiments forced by MII-induced SST anomalies

To further examine how the MII index represents El Niño Modoki II events, we perform the numerical simulations by using CAM4. Control run and two sensitivity experiments

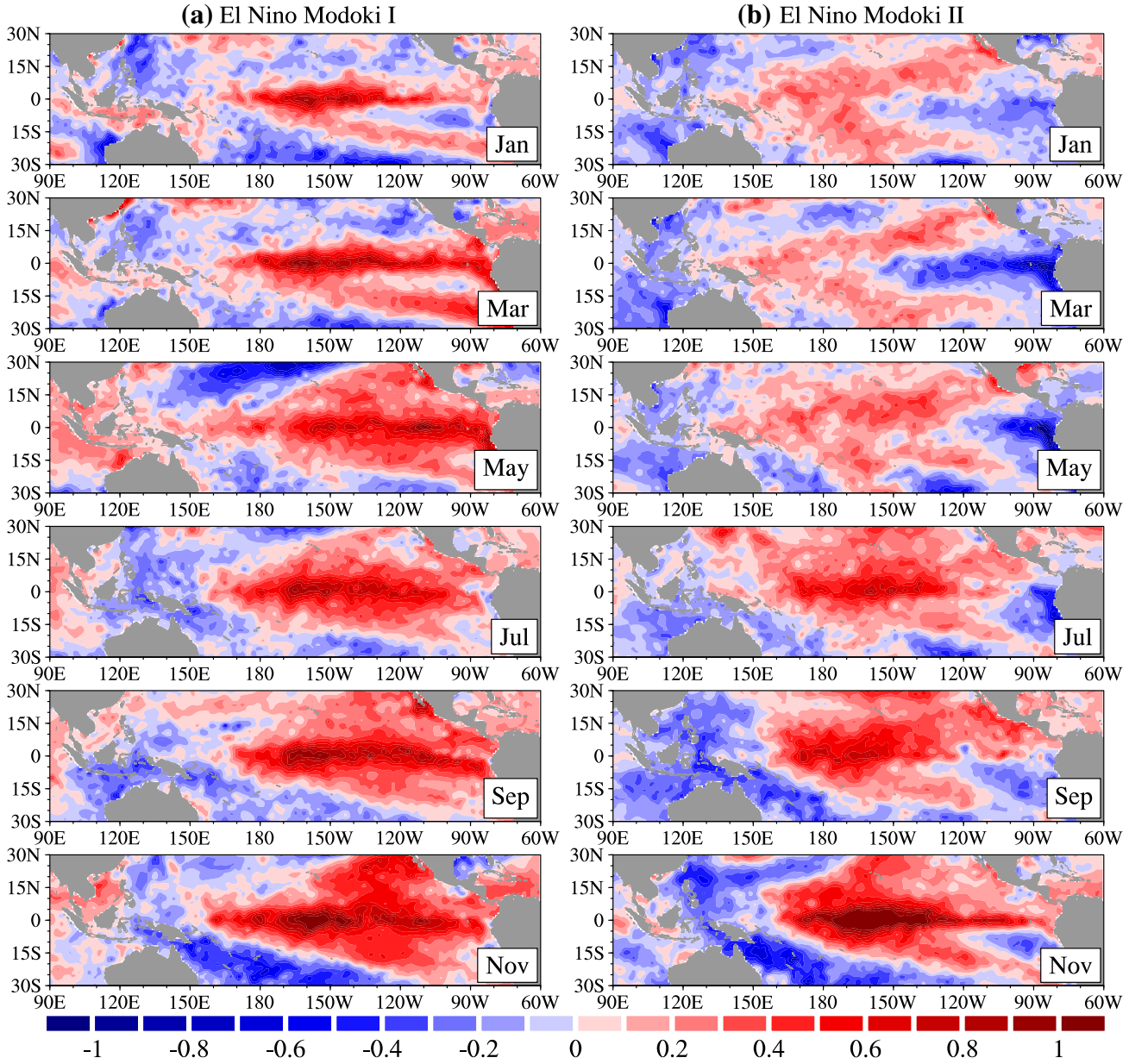

Fig. 9 Composited SST anomalies (°C) during El Niño Modoki I (**a**; *left column*) and El Niño Modoki II (**b**; *right column*), which are used to drive the sensitivity experiments. The El Niño years are selected from Table 4. The only odd months are shown

are conducted in the study. The control run is a 32-year integration forced by the climatological mean SST, and the last 30 years simulation results are composited as the climatology. In the two sensitivity experiments, the composited SST anomalies (Fig. 9) in the tropical Pacific (120°E–80°W, 30°S–30°N) for the identified El Niño Modoki I and II events during from January to December are imposed to the climatological SST to drive CAM4 for 16 years. The ensemble mean of last 10 years results are used to examine the responses of large-scale circulations to the identified El Niño Modoki I and II.

The model results reveal an anomalous cyclone circulation over east of the Philippines associated with a weakened SLP in El Niño Modoki II autumn, along with an anomalous anticyclone circulation in the west of the Philippines (Fig. 10b). Therefore, northerly wind anomalies are induced between such anomalous cyclone and anticyclone. Compared with the observed results [Figs. 2, 5c in Wang and Wang (2013)], the simulated northerly anomalies are farther eastward (Fig. 10b). Influenced by the northeasterly anomalies, the precipitation in southern China is reduced during El Niño Modoki II events although the negative rainfall anomalies also shift eastward (Fig. 11b). Nevertheless, the model results can well capture the basic atmospheric responses to El Niño Modoki II events (Wang and Wang 2013; Tan et al. 2016). Furthermore, for El Niño Modoki I, the simulated results are in good agreement with Wang and Wang (2013), showing an anomalous anticyclone near the Philippine Sea, southwesterly anomalies over the SCS (Fig. 10a) and increased precipitation in southern China (Fig. 11a). These model results provide credence in the MII index constructed in this study.

6 Summary and discussion

Based on different influences on precipitation in southern China during autumn, Wang and Wang (2013) divided El Niño Modoki into El Niño Modoki I and II. El Niño Modoki I is characterized by the anomalous warm SST originating in the central tropical Pacific. However, for El Niño Modoki II, anomalous warm SST emerges in the subtropical northeastern Pacific initially, and gradually extends to the central tropical Pacific. These distinct spatial patterns of SST anomalies give rise to different atmospheric responses. The anticyclone circulation anomalies emerge over the western North Pacific during boreal autumn of El Niño Modoki I, which resembles to that for canonical El Niño. The anticyclone results in negative relative vorticity anomalies in the western North Pacific. Different from that in El Niño Modoki I, an anomalous cyclone circulation appears in El Niño Modoki II, thus the positive vorticity anomalies are in the western North Pacific. Based on

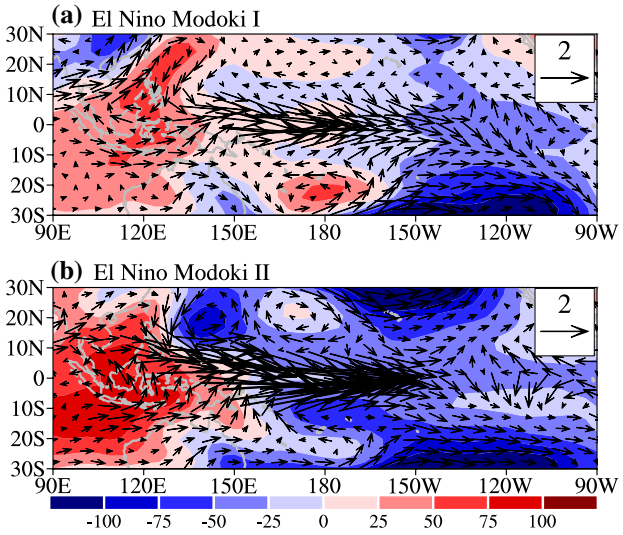

Fig. 10 Simulated wind anomalies at 850 hPa (*vector*; m s^{-1}) and SLP anomalies (*shading*; Pa) in autumn of El Niño Modoki I (**a**) and II (**b**) by CAM4

these ocean–atmosphere features, we perform an MV-EOF analysis of the EMI, Niño4 index along with the averaged 850 hPa relative vorticity anomalies in the Philippine Sea during boreal autumn. The first mode is defined as the El Niño Modoki II (MII) index, which shows the following features:

1. The MII index is highly correlated with the N_{WP} index and EMI, and the relationship with the Niño3 index is relatively weak.
2. The MII index has significant variations on interdecadal timescales (10–20 years) and interannual timescales (2–3 and 4–5 years).
3. Partial correlation analyses of the MII index removing the impacts of Niño3 and EMI can capture the major ocean–atmosphere features during the developing phase of El Niño Modoki II.
4. Forced by the El Niño Modoki II SST anomalies using the MII index, the model can well reproduce the atmospheric responses.

These results indicate that the constructed MII index can capture the coupled ocean–atmosphere features of El Niño Modoki II and can thus be used to describe El Niño Modoki II events.

El Niño largely affects climate and extreme weather events. Because various types of El Niño events show different climate impacts, it is important to identify the types of El Niño events. El Niño Modoki events need to be further divided into El Niño Modoki I and II because their influences on southern China rainfall and typhoon landfall in China as well as the IOD mode are opposite. The

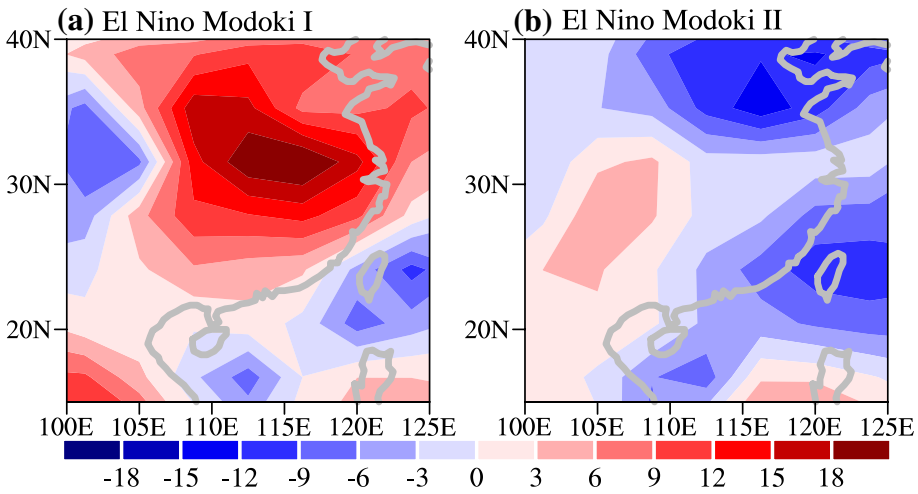

Fig. 11 Simulated rainfall anomalies (mm month^{-1}) in southern China during autumn of El Niño Modoki I (**a**) and II (**b**) by CAM4

influences of El Niño Modoki I and canonical El Niño are similar. For example, canonical El Niño and El Niño Modoki I induce negative rainfall anomalies in southern China during autumn, whereas El Niño Modoki II produces more rainfall than normal in southern China.

The constructed MII index can help us identify the various types of El Niño events. There are many methods identifying canonical El Niño and El Niño Modoki [see the recent papers by Capotondi et al. (2015) and Wang et al. (2016)]. All of El Niño Modoki events, including El Niño Modoki I and II, can be first identified by the EMI index, and other events are canonical El Niño (or selected from the Niño3 index). El Niño Modoki II events can be selected by the MII index. Subtracting El Niño Modoki II events from all of El Niño Modoki events, the rest are El Niño Modoki I events. By doing so, the three types of El Niño events can be identified.

The new constructed MII index developed in this paper provides a useful method and tool to study ENSO and ENSO's impacts through analyzing both observational data and model simulations. In addition, the constructed MII index can be applied in operational system as well as other ENSO indices to further improve ENSO and climate predictions. It is no doubt that the identification of El Niño Modoki II events will help improve predictions of rainfall in southern China and typhoon landfall in China during autumn of El Niño Modoki years. It is also useful to predict El Niño impacts on Indian Ocean climate. Knowing the types of El Niño events will also help project impacts of El Niño on climate and extreme events under global warming.

Acknowledgements This work was supported by the Strategic Priority Research Program of the Chinese Academy of Sciences (Grant No. XDA11010403), the CAS/SAFEA International Partnership Program for Creative Research Teams, the National Natural Science Foundation of China (Grant Nos. 41422601, 41376025 and 41521005), the Pioneer Hundred Talents Program of the Chinese Academy of Sciences, the National Basic Research Program of China (2013CB430301), the National Program on Global Change and Air–Sea Interaction (GASIIPOVAI-04).

Appendix

As a common statistical method, the correlation analysis is used to measure the correlativity of two variables (A_1 and A_2). The correlation coefficient (r_{12}) between A_1 and A_2 is calculated as

$$r_{12} = \frac{\sum_{i=1}^{n}\left(A_{1i}-\bar{A}_1\right)\left(A_{2i}-\bar{A}_2\right)}{\sqrt{\sum_{i=1}^{n}\left(A_{1i}-\bar{A}_1\right)^2}\sqrt{\sum_{i=1}^{n}\left(A_{2i}-\bar{A}_2\right)^2}} \tag{2}$$

where n is the sample size in the time series, $\bar{A}_1$ and $\bar{A}_2$ are the mean values of the two variables.

Given multiple time series, one time series may be affected by others. In this situation, the partial correlation is more appropriate. Assuming A_1 and A_2 are both correlated with the third variable (A_3), in order to remove the influence of A_3, the partial correlation coefficient ($r_{12,3}$) between A_1 and A_2 is defined as

$$r_{12,3} = \frac{r_{12}-r_{13}r_{23}}{\sqrt{(1-r_{13}^2)(1-r_{23}^2)}} \tag{3}$$

where r_{ij} is the correlation coefficient between A_i and A_j.

If A_1 and A_2 are both correlated with the other two variables (A_3 and A_4), thus the partial correlation coefficient between A_1 and A_2 ($r_{12,34}$) is described as

$$r_{12,34} = \frac{r_{12,4}-r_{13,4}r_{23,4}}{\sqrt{(1-r_{13,4}^2)(1-r_{23,4}^2)}} \tag{4}$$

where $r_{ij,k}$ is the partial correlation coefficient between A_i and A_j after removing the influence of A_k.

The corresponding statistical test is performed using Student's *t* test. The *t*-statistic (t) is defined in the form of

$$t = \frac{r\sqrt{n-q-2}}{\sqrt{1-r^2}} \tag{5}$$

where r is the (partial) correlation coefficient, n is the sample size, and q is the number of variables upon which we are conditioning. In this paper, we consider two variables, thus q is equal to 2. It should be noted that q is equal to 0 for the normal correlation analysis.

References

Alexander M, Bladé I, Newman M, Lanzante J, Lau NC, Scott J (2002) The atmospheric bridge: the influence of ENSO teleconnections on air–sea interaction over the global oceans. J Clim 15:2205–2231

Ashok K, Behera SK, Rao SA, Weng H, Yamagata T (2007) El Niño Modoki and its possible teleconnection. J Geophys Res 112:C11007. doi:10.1029/2006JC003798

Bjerknes J (1966) A possible response of the atmospheric Hadley circulation to equatorial anomalies of ocean temperature. Tellus 18:820–829

Bjerknes J (1969) Atmospheric teleconnections from the equatorial Pacific. Mon Weather Rev 97:163–172

Braganza K, Gergis JL, Power SB, Risbey JS, Fowler AM (2009) A multiproxy index of the El Niño–Southern Oscillation, AD 1525–1982. J Geophys Res Atmos 114:D05106. doi:10.1029/2008JD010896

Capotondi A et al (2015) Understanding ENSO diversity. Bull Am Meteorol Soc 96:921–938

Chiodi AM, Harrison DE (2013) El Niño impacts on seasonal US atmospheric circulation, temperature, and precipitation anomalies: the OLR-event perspective. J Clim 26:822–837

Cobb KM, Charles CD, Cheng H, Edwards RL (2003) El Niño/Southern Oscillation and tropical Pacific climate during the last millennium. Nature 424:271–276

Compo GP et al (2011) The twentieth century reanalysis project. Q J R Meteorol Soc 137:1–28

Dee DP et al (2011) The ERA-Interim reanalysis: configuration and performance of the data assimilation system. Q J R Meteorol Soc 137:553–597

Delcroix T, Picaut J (1998) Zonal displacement of the western equatorial Pacific "fresh pool". J Geophys Res Oceans 103(C1):1087–1098

Di Lorenzo E, Cobb KM, Furtado JC, Schneider N, Anderson BT, Bracco A, Alexander MA, Vimont DJ (2010) Central pacific El Niño and decadal climate change in the North Pacific ocean. Nat Geosci 3:762–765

Gent PR et al (2011) The community climate system model version 4. J Clim 24:4973–4991

Gergis J, Fowler A (2005) Classification of synchronous oceanic and atmospheric El Niño–Southern Oscillation (ENSO) events for palaeoclimate reconstruction. Int J Climatol 25:1541–1565

Hong CC, Li YH, Li T, Lee MY (2011) Impacts of central Pacific and eastern Pacific El Niños on tropical cyclone tracks over the western North Pacific. Geophys Res Lett 38:L16712. doi:10.1029/2011GL048821

Jin FF (1997) An equatorial ocean recharge paradigm for ENSO. Part I: conceptual model. J Atmos Sci 54:811–829

Kalnay E et al (1996) The NCEP/NCAR 40-year reanalysis project. Bull Am Meteorol Soc 77:437–471

Kao H, Yu J (2009) Contrasting eastern-Pacific and central-Pacific types of ENSO. J Clim 22:615–632

Kim JS, Zhou W, Wang X, Jain S (2012) El Niño Modoki and the summer precipitation variability over South Korea: a diagnostic study. J Meteorol Soc Jpn 90:673–684

Kug JS, Jin FF, An SI (2009) Two types of El Niño events: cold tongue El Niño and warm pool El Niño. J Clim 22:1499–1515

Larkin NK, Harrison DE (2005) Global seasonal temperature and precipitation anomalies during El Niño autumn and winter. Geophys Res Lett 32:L16705. doi:10.1029/2005GL022860

Lee T, McPhaden MJ (2010) Increasing intensity of El Niño in the central-equatorial Pacific. Geophys Res Lett 37:L14603. doi:10.1029/2010GL044007

Liu QY, Wang D, Wang X, Shu Y, Xie Q, Chen J (2014) Thermal variations in the South China Sea associated with the eastern and central Pacific El Niño events and their mechanisms. J Geophys Res Oceans 119:8955–8972

Neale RB, Richter J, Park S, Lauritzen PH, Vavrus SJ, Rasch PJ, Zhang M (2013) The mean climate of the community atmosphere model (CAM4) in forced SST and fully coupled experiments. J Clim 26:5150–5168

North GR, Bell TL, Cahalan RF, Moeng FJ (1982) Sampling errors in the estimation of empirical orthogonal functions. Mon Weather Rev 110:699–706

Picaut J, Ioualalen M, Delcroix T, Masia F, Murtugudde R, Vialard J (2001) The oceanic zone of convergence on the eastern edge of the Pacific warm pool: a synthesis of results and implications for El Niño Southern Oscillation and biogeochemical phenomena. J Geophys Res Oceans 106(C2):2363–2386

Qu T, Yu JY (2014) ENSO indices from sea surface salinity observed by Aquarius and Argo. J Oceanogr 70:367–375

Rasmusson EM, Carpenter TH (1982) Variations in tropical sea surface temperature and surface wind fields associated with the Southern Oscillation/El Niño. Mon Weather Rev 110:354–384

Rayner NA, Parker DE, Horton EB, Folland CK, Alexander LV, Rowell DP, Kent EC, Kaplan A (2003) Global analysis of sea surface temperature, sea ice and night marine air temperature since the late nineteenth century. J Geophys Res Atmos 108:4407. doi:10.1029/2002JD002670

Ren HL, Jin FF (2011) Niño indices for two types of ENSO. Geophys Res Lett 38:L04704. doi:10.1029/2010GL046031

Ropelewski CF, Jones PD (1987) An extension of the Tahiti–Darwin southern oscillation index. Mon Weather Rev 115:2161–2165

Schneider U, Becker A, Finger P, Meyer-Christoffer A, Rudolf B, Ziese M (2011) GPCC full data reanalysis version 6.0 at 1.0°: monthly land-surface precipitation from rain-gauges built on GTS-based and historic data. doi:10.5676/DWD_GPCC/FD_M_V6_100

Singh A, Delcroix T, Cravatte S (2011) Contrasting the flavors of El Niño and Southern Oscillation using sea surface salinity observations. J Geophys Res Oceans 116:C06016. doi:10.1029/2010JC006862

Takahashi K, Montecinos A, Goubanova K, Dewitte B (2011) ENSO regimes: reinterpreting the canonical and Modoki El Niño. Geophys Res Lett 38:L10704

Tan W, Wang X, Wang W, Wang C, Zuo J (2016) Different responses of sea surface temperature in the South China Sea to various El Niño events during Boreal Autumn. J Clim 29:1127–1142

Trenberth KE (1997) The definition of El Niño. Bull Am Meteorol Soc 78:2771–2777

Trenberth KE, Stepaniak DP (2001) Indices of El Niño evolution. J Clim 14:1697–1701

Wang B (1992) The vertical structure and development of the ENSO anomaly mode during 1979–1989. J Atmos Sci 49:698–712

Wang C (2002) Atmospheric circulation cells associated with the El Niño–Southern Oscillation. J Clim 15:399–419

Wang B, Wang Y (1994) Development of El Niños during 1971–1992. Trans Oceanol Limnol 2:26–40

Wang C, Wang X (2013) Classifying El Niño Modoki I and II by different impacts on rainfall in Southern China and typhoon tracks. J Clim 26:1322–1338

Wang X, Wang C (2014) Different impacts of various El Niño events on the Indian Ocean Dipole. Clim Dyn 42:991–1005

Wang B, Wu R, Fu X (2000) Pacific–East Asian teleconnection: how does ENSO affect East Asian climate? J Clim 13:1517–1536

Wang B, Wu Z, Li J, Liu J, Chang CP, Ding Y, Wu G (2008) How to measure the strength of the East Asian summer monsoon. J Clim 21:4449–4463

Wang X, Zhou W, Li C, Wang D (2014) Comparison of the impact of two types of El Niño on tropical cyclone genesis over the South China Sea. Int J Climatol 34:2651–2660. doi:10.1002/joc.3865

Wang C, Deser C, Yu JY, DiNezio P, Clement A (2016) El Niño–Southern Oscillation (ENSO): a review. In: Coral Reefs of the Eastern Pacific, Glymn P, Manzello D, Enochs I (eds). Springer Science Publisher, Berlin, pp 85–106

Weisberg RH, Wang C (1997) A western Pacific oscillator paradigm for the El Niño–Southern Oscillation. Geophys Res Lett 24:779–782

Weng H, Ashok K, Behera SK, Rao SA, Yamagata T (2007) Impacts of recent El Niño Modoki on dry/wet conditions in the Pacific Rim during boreal summer. Clim Dyn 29:113–129

Wolter K, Timlin MS (1993) Monitoring ENSO in COADS with a seasonally adjusted principal component index. In: Proc of the 17th climate diagnostics workshop, pp 52–57

Wolter K, Timlin MS (2011) El Niño/Southern Oscillation behaviour since 1871 as diagnosed in an extended multivariate ENSO index (MEI.ext). Int J Climatol 31:1074–1087

Xu K, Zhu C, He J (2012) Linkage between the dominant modes in Pacific subsurface ocean temperature and the two type ENSO events. Chin Sci Bull 57:3491–3496

Yeh SW, Kug JS, Dewitte B, Kwon MH, Kirtman BP, Jin FF (2009) El Niño in a changing climate. Nature 461:511–514

Yeh SW, Wang X, Wang CZ, Dewitte B (2015) On the relationship between the North Pacific climate variability and the central Pacific El Niño. J Clim 28:663–677

Yu JY, Kim ST (2011) Relationships between extratropical sea level pressure variations and the central Pacific and eastern Pacific types of ENSO. J Clim 24:708–720

Yu JY, Kao HY, Lee T (2010) Subtropics-related interannual sea surface temperature variability in the central equatorial Pacific. J Clim 23:2869–2884

Yu JY, Kao HY, Lee T, Kim ST (2011) Subsurface ocean temperature indices for Central-Pacific and Eastern-Pacific types of El Niño and La Niña events. Theor Appl Climatol 103:337–344

Yu JY, Lu MM, Kim ST (2012) A change in the relationship between tropical central Pacific SST variability and the extratropical atmosphere around 1990. Environ Res Lett 7:034025